JOURNAL OF GUIDANCE, CONTROL, AND DYNAMICS
Vol. 31, No. 5, September–October 2008

Six-Degree-of-Freedom Trajectory Optimization Using a Two-Timescale Collocation Architecture

Prasun N. Desai*
NASA Langley Research Center, Hampton, Virginia 23681
and
Bruce A. Conway†
University of Illinois, Urbana, Illinois 61801

DOI: 10.2514/1.34020

Six-degree-of-freedom trajectory optimization of a reentry vehicle is performed using a two-timescale collocation methodology. This class of six-degree-of-freedom trajectory problems is characterized by two distinct timescales in their governing equations, in which a subset of the states have high-frequency dynamics (the rotational equations of motion), whereas the remaining states (the translational equations of motion) vary comparatively slowly. With conventional collocation methods, the six-degree-of-freedom problem becomes extraordinarily large and the problem becomes difficult to solve. Using the two-timescale collocation architecture, the problem size is reduced significantly. The converged solution shows a realistic landing profile and captures the appropriate high-frequency rotational dynamics. A large reduction in the overall problem size (by 55%) is attained with the two-timescale architecture as compared to the conventional single-timescale collocation method. Consequently, optimum six-degree-of-freedom trajectories can now be found efficiently using collocation, which was not previously possible for a system with two distinct timescales in the governing states.

Nomenclature

C_D = drag force coefficient
C_L = lift force coefficient
C_l = rolling moment coefficient
C_m = pitching moment coefficient
C_n = yawing moment coefficient
C_Y = side force coefficient
D = total drag force $= 0.5\rho V^2 S C_D$
g = μ/r^2
h = altitude
I = inertia matrix
L = total lift force $= 0.5\rho V^2 S C_L$
l = reference length
M_x = total rolling moment $= 0.5\rho V^2 S l C_l$
M_y = total pitching moment $= 0.5\rho V^2 S l C_m$
M_z = total yawing moment $= 0.5\rho V^2 S l C_n$
m = vehicle mass
R = radius of Earth
r = radius $= (R + h)$
S = vehicle reference area
V = velocity
Y = total side force $= 0.5\rho V^2 S C_Y$
α = angle of attack
β = sideslip angle
γ = flight-path angle
λ = longitude
μ = gravitational parameter of Earth
ρ = atmospheric density
σ = bank angle
ϕ = latitude
ψ = azimuth (+clockwise from north)

Presented at the 2005 AAS/AIAA Astrodynamics Specialists Conference, Lake Tahoe, CA, 7–11 August 2005; received 13 August 2007; revision received 30 March 2008; accepted for publication 6 April 2008.

*Senior Aerospace Engineer, Atmospheric Flight and Entry Systems Branch, 1 North Dryden Street, Mail Stop 489; prasun.n.desai@nasa.gov. Associate Fellow AIAA.

†Professor, Department of Aerospace Engineering, 306 Talbot Laboratory; bconway@uiuc.edu. Associate Fellow AIAA.

I. Introduction

COLLOCATION with nonlinear programming (NLP) has been used extensively to solve a variety of three-degree-of-freedom trajectory (3DOF) optimization problems (e.g., aircraft or spacecraft trajectories in which only the translational equations of motion are considered). However, solving six-degree-of-freedom (6DOF) trajectory optimization problems (i.e., problems in which the coupled translational and rotational equations of motion are considered) using collocation has seldom been attempted. The problem that arises is that 6DOF problems are characterized by having two distinct timescales in the system states. That is, a subset of the states has high-frequency dynamics (rotational equations of motion), whereas the remaining states (translational equations of motion) vary comparatively slowly.

In conventional or standard collocation, a single-timescale discretization scheme is used for all the state variables [1]. Thus, the timescale for the discretization in a 6DOF problem is set by the need to capture the high-frequency rotational dynamics, and so the width of the time segments into which the total time is divided becomes quite small. Even if only one state variable requires a small discretization timescale, all the state variables must use a small timescale. Because every state variable at every segment boundary (node) is an NLP parameter, an extraordinarily large nonlinear programming problem results. In addition, the 6DOF problem is naturally much larger, because there are 13 system differential equations compared to only six for a 3DOF simulation. The resulting CPU time required for the solution grows correspondingly. Moreover, the governing equations for 6DOF problems are highly coupled and highly nonlinear, adding further difficulty in attaining a converged solution due to the increased sensitivity of the solution to the initial guess. Consequently, very large problems that result from transcribing a 6DOF problem using conventional collocation can prove very difficult to solve.

To overcome this difficulty, a much more efficient two-timescale collocation discretization scheme has been employed [2,3]. This two-timescale collocation method allows the use of a coarser

discretization in time for the smoothly varying (low-frequency) state equations, and a second finer discretization in time that can be used for the higher-frequency state equations. Consequently, the finer discretization timescale can be applied to only those state variables that have higher-frequency dynamics in the governing equations, whereas the rest of the state variables can use a much coarser discretization timescale. This two-timescale methodology is well suited for solving 6DOF trajectory optimization problems, where the dynamics characterized by the translational motion state variables are at a low frequency, whereas the dynamics characterized by the rotational motion state variables are at a high frequency. This approach allows the size of the overall optimization problem to be reduced significantly.

Desai and Conway [2,3] describe in detail the development of the two-timescale collocation architecture. Two different two-timescale discretization schemes are presented: 1) using two segments to represent the high-frequency state variables for every one segment of the low-frequency state variables (i.e., a two-to-one discretization architecture), and 2) using four segments to represent the high-frequency state variables for every one segment of the low-frequency state variables (i.e., a four-to-one discretization architecture). This paper presents the results of employing the two-timescale collocation discretization scheme to solve a 6DOF trajectory optimization problem for the approach and landing trajectory for the HL-20 lifting body vehicle shown in Fig. 1 [4,5]. The four-to-one discretization architecture is used in this analysis.

II. Six-Degree-of-Freedom Equations of Motion

The equations of motion for the six-degree-of-freedom trajectory of an unpowered flight vehicle are first presented [6,7]. The translational equations of motion are referenced to a flight-path coordinate system, whereas the rotational equations of motion are referenced to a vehicle-body-fixed coordinate system.

A. Translational Equations of Motion

The translational equations of motion are described by six first-order time rate of change equations:

$$\frac{\mathrm{d}h}{\mathrm{d}t} = V\sin\gamma \tag{1}$$

$$\frac{\mathrm{d}\phi}{\mathrm{d}t} = \frac{V\cos\gamma\cos\psi}{r} \tag{2}$$

$$\frac{\mathrm{d}\lambda}{\mathrm{d}t} = \frac{V\cos\gamma\sin\psi}{r\cos\phi} \tag{3}$$

$$\frac{\mathrm{d}V}{\mathrm{d}t} = \frac{1}{m}(Y\sin\beta - D\cos\beta) - g\sin\gamma + \Omega^2 r\cos\phi(\sin\gamma\cos\phi - \cos\gamma\sin\phi\cos\psi) \tag{4}$$

$$\frac{\mathrm{d}\gamma}{\mathrm{d}t} = \frac{1}{mV}(L\cos\sigma - D\sin\beta\sin\sigma - Y\cos\beta\sin\sigma) + \left(\frac{V}{r} - \frac{g}{V}\right)\cos\gamma + 2\Omega\cos\phi\sin\psi + \frac{\Omega^2 r}{V}\cos\phi(\cos\gamma\cos\phi + \sin\gamma\sin\phi\cos\psi) \tag{5}$$

$$\frac{\mathrm{d}\psi}{\mathrm{d}t} = \frac{1}{mV\cos\gamma}(L\sin\sigma + D\sin\beta\cos\sigma + Y\cos\beta\cos\sigma) + \frac{V\cos\gamma}{r}\sin\psi\tan\phi - 2\Omega(\cos\phi\cos\psi\tan\gamma - \sin\phi) + \frac{\Omega^2 r}{V\cos\gamma}\cos\phi\sin\phi\sin\psi \tag{6}$$

B. Rotational Equations of Motion

The rotational equations of motion are described by seven first-order time rate of change equations [Eqs. (7) and (8)]:

$$\frac{\mathrm{d}\bar{\omega}}{\mathrm{d}t} = I^{-1}[\Sigma\bar{M} - \bar{\omega}\times I\bar{\omega}] \tag{7}$$

$$\frac{\mathrm{d}\bar{e}}{\mathrm{d}t} = \frac{1}{2}[\omega]\bar{e} \tag{8}$$

where $\bar{\omega}$ = angular velocity of vehicle expressed in vehicle-body-fixed coordinates (i.e., about roll, pitch, and yaw axes), $\bar{e}$ = four-dimensional vector of quaternion parameters [8,9], and $\bar{M}$ = external moments acting on vehicle expressed in vehicle-body-fixed coordinates (i.e., about roll, pitch, and yaw axes). That is,

$$I = \begin{bmatrix} I_{xx} & I_{xy} & I_{xz} \\ I_{xy} & I_{yy} & I_{yz} \\ I_{xz} & I_{yz} & I_{zz} \end{bmatrix}, \qquad \bar{\omega} = \begin{bmatrix} \omega_x \\ \omega_y \\ \omega_z \end{bmatrix}, \qquad \bar{M} = \begin{bmatrix} M_x \\ M_y \\ M_z \end{bmatrix}$$

$$[\omega] = \begin{bmatrix} 0 & \omega_z & -\omega_y & \omega_x \\ -\omega_z & 0 & \omega_x & \omega_y \\ \omega_y & -\omega_x & 0 & \omega_z \\ -\omega_x & -\omega_y & -\omega_z & 0 \end{bmatrix}$$

where the quaternion vector $\bar{e}$ must satisfy the constraint that the sum of its squared components be equal to unity (e_4 is scalar term):

$$e_1^2 + e_2^2 + e_3^2 + e_4^2 = 1$$

The body angular rates ω_x, ω_y, ω_z, and external moments M_x, M_y, M_z, are illustrated in Fig. 2. The matrix $[\omega]$ is referred to as a skew-symmetric matrix.

The complete set of 6DOF equations of motion is defined by Eqs. (1–8). The translational Eqs. (1–6) and rotational Eqs. (7) and (8) are coupled through the aerodynamic forces (D, L, Y) and

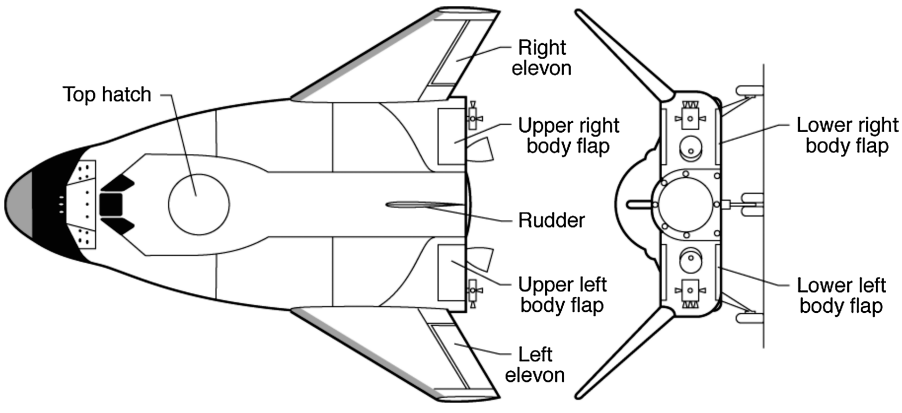

Fig. 1 HL-20 configuration.

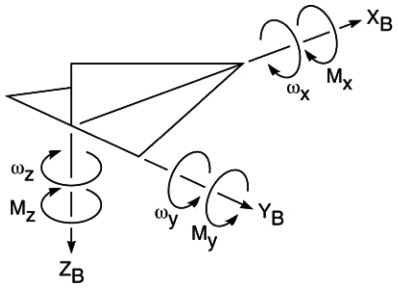

Fig. 2 Orientation of vehicle body axes and angular rates.

moments (M_x, M_y, M_z). Equations (7) and (8) define the vehicle attitude and attitude rates, which determine the vehicle aerodynamic coefficients, which in turn affect the translational motion of the vehicle [Eqs. (1–6)].

The total aerodynamic drag D, lift L, and side Y forces, and rolling M_x, pitching M_y, and yawing M_z moments are functions of the Mach number M, angle of attack α, sideslip angle β, and the deflections of the control surfaces of the HL-20 vehicle: upper left and right body flaps ($\delta_{\text{bf}_{\text{ul}}}, \delta_{\text{bf}_{\text{ur}}}$), lower left and right body flaps ($\delta_{\text{bf}_{\text{ll}}}, \delta_{\text{bf}_{\text{lr}}}$), left and right elevon ($\delta_{\text{elvn}_l}, \delta_{\text{elvn}_r}$), and the rudder ($\delta_{\text{rudder}}$). That is,

$$
\begin{aligned}
D &= f(M, \alpha, \beta, \delta_{\text{bf}_{\text{ul}}}, \delta_{\text{bf}_{\text{ur}}}, \delta_{\text{bf}_{\text{ll}}}, \delta_{\text{bf}_{\text{lr}}}, \delta_{\text{elvn}_l}, \delta_{\text{elvn}_r}, \delta_{\text{rudder}}) \\
L &= f(M, \alpha, \beta, \delta_{\text{bf}_{\text{ul}}}, \delta_{\text{bf}_{\text{ur}}}, \delta_{\text{bf}_{\text{ll}}}, \delta_{\text{bf}_{\text{lr}}}, \delta_{\text{elvn}_l}, \delta_{\text{elvn}_r}, \delta_{\text{rudder}}) \\
Y &= f(M, \alpha, \beta, \delta_{\text{bf}_{\text{ul}}}, \delta_{\text{bf}_{\text{ur}}}, \delta_{\text{bf}_{\text{ll}}}, \delta_{\text{bf}_{\text{lr}}}, \delta_{\text{elvn}_l}, \delta_{\text{elvn}_r}, \delta_{\text{rudder}}) \\
M_x &= f(M, \alpha, \beta, \delta_{\text{bf}_{\text{ul}}}, \delta_{\text{bf}_{\text{ur}}}, \delta_{\text{bf}_{\text{ll}}}, \delta_{\text{bf}_{\text{lr}}}, \delta_{\text{elvn}_l}, \delta_{\text{elvn}_r}, \delta_{\text{rudder}}) \\
M_y &= f(M, \alpha, \beta, \delta_{\text{bf}_{\text{ul}}}, \delta_{\text{bf}_{\text{ur}}}, \delta_{\text{bf}_{\text{ll}}}, \delta_{\text{bf}_{\text{lr}}}, \delta_{\text{elvn}_l}, \delta_{\text{elvn}_r}, \delta_{\text{rudder}}) \\
M_z &= f(M, \alpha, \beta, \delta_{\text{bf}_{\text{ul}}}, \delta_{\text{bf}_{\text{ur}}}, \delta_{\text{bf}_{\text{ll}}}, \delta_{\text{bf}_{\text{lr}}}, \delta_{\text{elvn}_l}, \delta_{\text{elvn}_r}, \delta_{\text{rudder}})
\end{aligned}
$$

The aerodynamic coefficients C_D, C_L, C_Y, C_l, C_m, and C_n needed to calculate D, L, Y, M_x, M_y, and M_z, respectively, are obtained from an aerodynamic database [10,11] and are a combination of the core vehicle coefficients without any control surface deflections plus contributions from deflecting the various control surfaces. Hence, all seven control surfaces contribute to the total aerodynamic forces and moments. The control surface deflection sign convention is shown in Fig. 3.

III. Problem Formulation

To demonstrate the capability of the two-timescale collocation discretization scheme to optimize 6DOF trajectory problems, the optimal HL-20 vehicle approach and landing problem is solved (Fig. 4). The four-to-one two-timescale scheme discretization architecture (i.e., using four segments to represent the high-frequency state variables for every one segment of the low-frequency state variables) is used as described in [2,3].

The objective function for this sample test problem is to minimize the velocity at touchdown, subject to the following constraints:

$$
0 \text{ deg} \le \alpha \le 15 \text{ deg} \qquad \frac{d\gamma}{dt} \ge 0 \qquad 0.98 \le |\bar{e}| \le 1.02
$$

$$
-1 \text{ m/s} \le V_f \sin\gamma_f \le 0 \text{ m/s}
$$

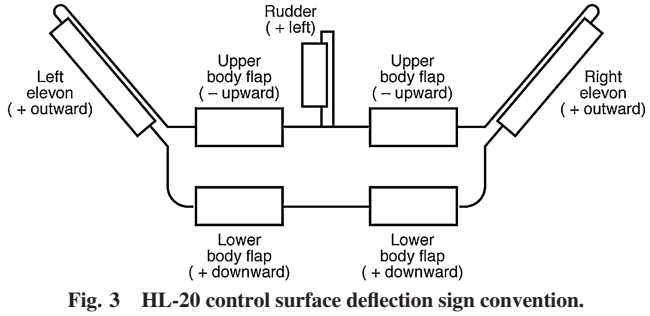

Fig. 3 HL-20 control surface deflection sign convention.

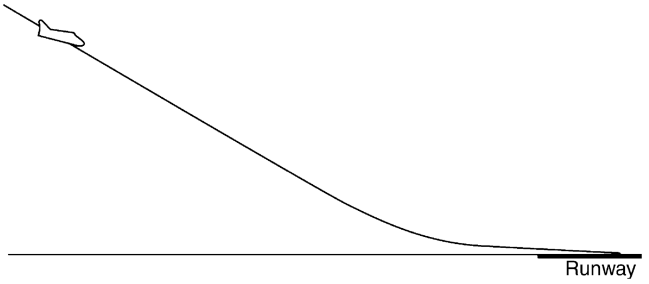

Fig. 4 Approach and landing geometry.

The first three constraints represent path constraints (imposed during the entire flight), where the angle of attack must always be less than 15 deg, the time derivative of the flight-path angle must always be positive (this constraint assures that the altitude always decreases), and the norm of the quaternion vector remains close to unity (this constraint assures the quaternion vector does not become inaccurate). Lastly, a terminal boundary constraint is imposed on the sink rate at touchdown to limit landing loads.

The upper and lower bounds on the state and control variables are as follows:

State variables

$$
\begin{aligned}
&0 \text{ m} \le h \le 10{,}000 \text{ m} && 0 \text{ deg} \le \phi \le 50 \text{ deg} \\
&0 \text{ deg} \le \lambda \le 50 \text{ deg} && 0.1 \text{ m/s} \le V \le 500 \text{ m/s} \\
&-90 \text{ deg} \le \gamma \le 0 \text{ deg} && 0 \text{ deg} \le \psi \le 180 \text{ deg} \\
&-5 \text{ deg/s} \le \omega_x \le 5 \text{ deg/s} && -5 \text{ deg/s} \le \omega_y \le 5 \text{ deg/s} \\
&-5 \text{ deg/s} \le \omega_z \le 5 \text{ deg/s} && \\
&-1.0 \le e_1 \le 1.0 && -1.0 \le e_2 \le 1.0 \\
&-1.0 \le e_3 \le 1.0 && -1.0 \le e_4 \le 1.0
\end{aligned}
$$

Control variables

$$
\begin{aligned}
&-60 \text{ deg} \le \delta_{\text{bf}_{\text{ul}}} \le 0 \text{ deg} && -60 \text{ deg} \le \delta_{\text{bf}_{\text{ur}}} \le 0 \text{ deg} \\
&0 \text{ deg} \le \delta_{\text{bf}_{\text{ll}}} \le 60 \text{ deg} && 0 \text{ deg} \le \delta_{\text{bf}_{\text{lr}}} \le 60 \text{ deg} \\
&-30 \text{ deg} \le \delta_{\text{elvn}_l} \le 30 \text{ deg} && -30 \text{ deg} \le \delta_{\text{elvn}_r} \le 30 \text{ deg} \\
&-30 \text{ deg} \le \delta_{\text{rudder}} \le 30 \text{ deg} &&
\end{aligned}
$$

The specified initial and final conditions are

$$
\begin{aligned}
&\phi(t_o) = 20 \text{ deg} && \phi(t_f) = 20.1 \text{ deg} \\
&\lambda(t_o) = 20 \text{ deg} && \lambda(t_f) = 20.1 \text{ deg} \\
&\psi(t_o) = 0 \text{ deg} && \psi(t_f) = 90 \text{ deg} \\
& && h(t_f) = 0 \text{ m}
\end{aligned}
$$

The mass and inertia properties for the HL-20 vehicle are

$$
m = 8664 \text{ kg} \qquad I_{xx} = 10{,}185 \text{ kg} \cdot \text{m}^2
$$

$$
I_{yy} = 45{,}547 \text{ kg} \cdot \text{m}^2 \qquad I_{zz} = 48{,}327 \text{ kg} \cdot \text{m}^2
$$

The optimal control problem was solved using the method of direct collocation with nonlinear programming. When using this method, there are many possibilities for the required implicit integration constraints [1,12,13]. This 6DOF sample test problem was transcribed into an NLP problem using the Gauss–Lobatto implicit integration constraint formulation [12]. In this formulation, the total time T is discretized into n segments of length $t = T/n$, where each state variable is represented by a quintic polynomial (in time) within each segment (Fig. 5). Six parameters are required to define the polynomial uniquely; the polynomial can be determined using the values of the states (x_i, x_{i+1}, x_{i+2}) at the segment boundaries and at the center point, together with the values of the time derivatives f_i, f_{i+1}, and f_{i+2}, which correspond to values of

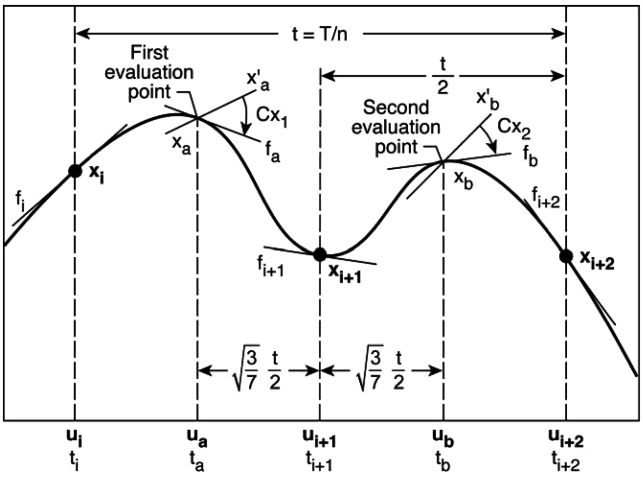

Fig. 5 Fifth-degree Gauss–Lobatto system constraint formulation.

dx/dt [Eqs. (1–8)] evaluated at t_i, t_{i+1}, and t_{i+2}, respectively. Note that evaluation of f_i, f_{i+1}, and f_{i+2} requires specification of the control variables at the same times (i.e., requires u_i, u_{i+1}, u_{i+2}). Making use of x_i, x_{i+1}, x_{i+2}, u_i, u_{i+1}, u_{i+2}, f_i, f_{i+1}, and f_{i+2}, a quintic polynomial representing the state time history between the endpoints can be constructed (as shown in Fig. 5).

In the collocation method using the fifth-degree Gauss–Lobatto polynomial, the quintic polynomial is forced to satisfy two additional constraints within each segment at the "collocation" points t_a and t_b (shown in Fig. 5). That is, at these two interior points t_a and t_b, the quintic polynomial must satisfy the system differential equations. The location of these two points is not arbitrary; no other choice of two such points yields a more precise implicit integration. The algebraic constraints take the form [12]

$$Cx_1 = f_a - x'_a = \frac{1}{360}[(32\sqrt{21} + 180)x_i - 64\sqrt{21}x_{i+1} + (32\sqrt{21} - 180)x_{i+2} + t\{(9 + \sqrt{21})f_i + 98f_a + 64f_{i+1} + (9 - \sqrt{21})f_{i+2}\}] = 0 \tag{9}$$

$$Cx_2 = f_b - x'_b = \frac{1}{360}[(-32\sqrt{21} + 180)x_i + 64\sqrt{21}x_{i+1} + (-32\sqrt{21} - 180)x_{i+2} + t\{(9 - \sqrt{21})f_i + 98f_b + 64f_{i+1} + (9 + \sqrt{21})f_{i+2}\}] = 0 \tag{10}$$

where $f_a = f(x_a, u_a, t_a)$ and $f_b = f(x_b, u_b, t_b)$. The constraints given in Eqs. (9) and (10) are termed the fifth-degree Gauss–Lobatto system constraints.

The states (x_i, x_{i+1}, x_{i+2}) and controls $(u_i, u_a, u_{i+1}, u_b, u_{i+2})$ shown in bold in Fig. 5 are discrete NLP parameters. The values of these states and controls are selected to force the algebraic constraints of Eqs. (9) and (10) to zero. In so doing, the polynomial is made to satisfy the differential equation at the collocation points t_a and t_b of the segment (in addition to being implicitly satisfied at t_i, t_{i+1}, and t_{i+2}). When Eqs. (9) and (10) are satisfied, an approximate solution to the system equations is obtained. The method is discussed in much greater detail in [12,14].

The nonlinear programming problem was solved using the sparse solver SNOPT [15]. The problem contains a total of 13 state variables. There are six states describing vehicle translation; these states are expected to have a smooth variation in time and experience only low-frequency change. There are seven states describing rotation of the vehicle about its center of mass; these states are expected to experience change at high frequency. This problem is thus a good candidate for solution using the two-timescale collocation architecture [2,3].

The translational state variables h, ϕ, λ, V, γ, ψ are defined as the low-frequency parameters, whereas the rotational state variables ω_x, ω_y, ω_z, e_1, e_2, e_3, e_4 are defined as the high-frequency parameters. There are seven control variables ($\delta_{\text{bf}_{\text{ul}}}$, $\delta_{\text{bf}_{\text{ur}}}$, $\delta_{\text{bf}_{\text{ll}}}$, $\delta_{\text{bf}_{\text{lr}}}$, δ_{elvn_l}, δ_{elvn_r}, δ_{rudder}). The "four-to-one" two-timescale discretization architecture is selected [2,3]. Thus, with the total time divided into 12 segments for the low-frequency state variables, 48 segments are required for the high-frequency variables.

The collocation method requires an initial guess of all of the discrete parameters that constitute the solution time history. The method is comparatively robust (i.e., it is capable of converging to a solution from a poor initial guess). The initial guess used for the state and control variable time histories for this problem was a linear interpolation in time between the following initial and final values:

$h_o = 5000$ m	$h_f = 0$ m
$\phi_o = 20$ deg	$\phi_f = 20.1$ deg
$\lambda_o = 20$ deg	$\lambda_f = 20.1$ deg
$V_o = 225$ m/s	$V_f = 100$ m/s
$\gamma_o = -10$ deg	$\gamma_f = -2$ deg
$\psi_o = 0$ deg	$\psi_f = 90$ deg
$\omega_{x_o} = 0.1$ deg/s	$\omega_{x_f} = 0$ deg/s
$\omega_{y_o} = 0.1$ deg/s	$\omega_{y_f} = 0$ deg/s
$\omega_{z_o} = 0.1$ deg/s	$\omega_{z_f} = 0$ deg/s
$e_{1_o} = 0.1$ rad	$e_{1_f} = 0.1$ rad
$e_{2_o} = 0.1$ rad	$e_{2_f} = 0.1$ rad
$e_{3_o} = 0.1$ rad	$e_{3_f} = 0.1$ rad
$e_{4_o} = 0.1$ rad	$e_{4_f} = 0.1$ rad
$\delta_{\text{bf}_{\text{ul}}o} = -10$ deg	$\delta_{\text{bf}_{\text{ul}}f} = -10$ deg
$\delta_{\text{bf}_{\text{ur}}o} = -10$ deg	$\delta_{\text{bf}_{\text{ur}}f} = -10$ deg
$\delta_{\text{bf}_{\text{ll}}o} = 10$ deg	$\delta_{\text{bf}_{\text{ll}}f} = 10$ deg
$\delta_{\text{bf}_{\text{lr}}o} = 10$ deg	$\delta_{\text{bf}_{\text{lr}}f} = 10$ deg
$\delta_{\text{elvn}_l o} = 10$ deg	$\delta_{\text{elvn}_l f} = 10$ deg
$\delta_{\text{elvn}_r o} = 10$ deg	$\delta_{\text{elvn}_r f} = 10$ deg

IV. Results

The results for the optimized solution are shown in Figs. 6–24. The landed velocity is 105.2 m/s. The solution to this sample test problem was reached through a succession of optimization cycles;

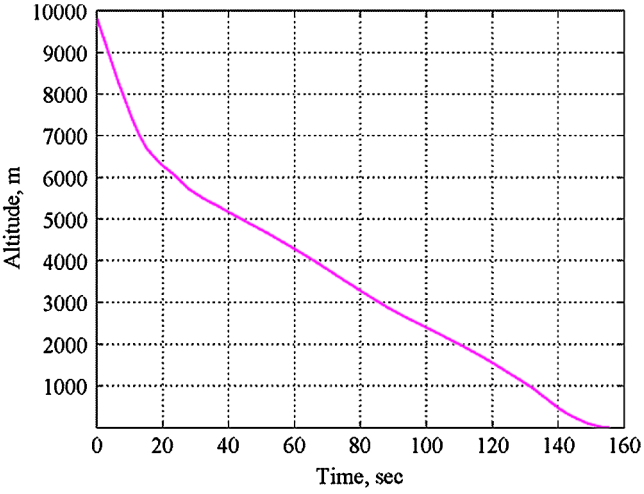

Fig. 6 Time history of altitude.

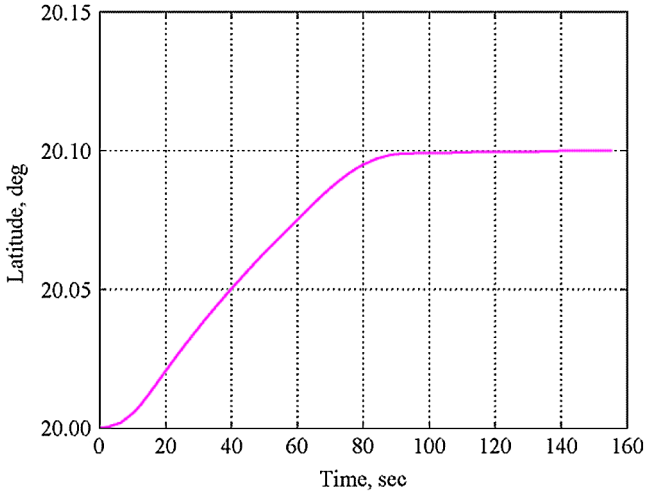

Fig. 7 Time history of latitude.

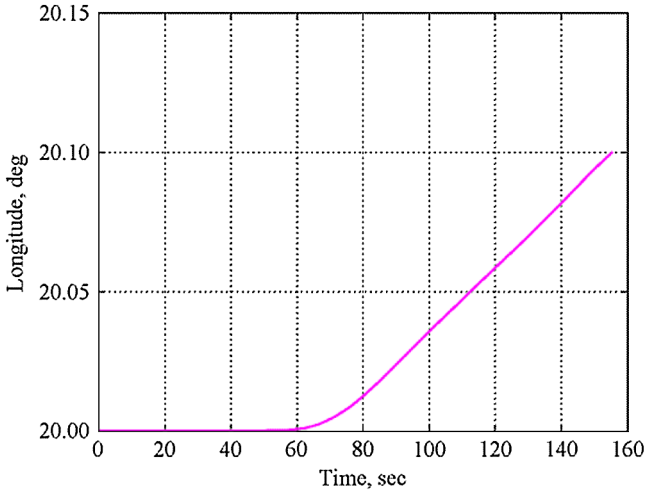

Fig. 8 Time history of longitude.

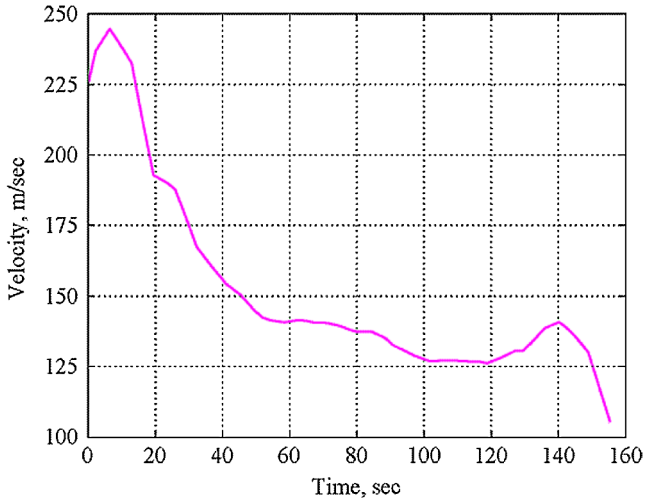

Fig. 9 Time history of velocity.

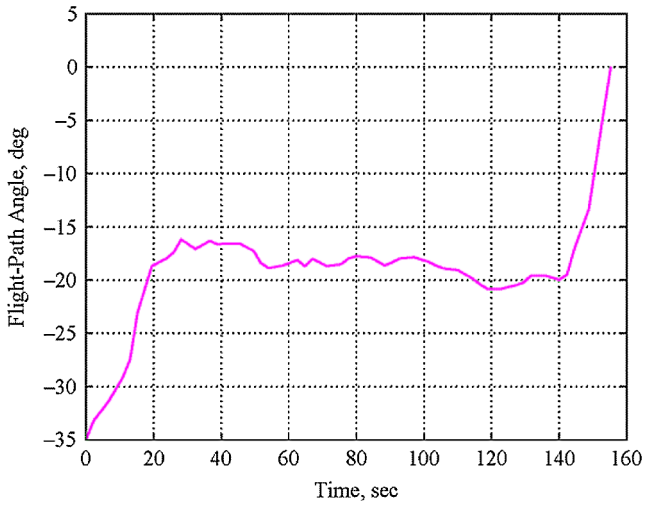

Fig. 10 Time history of flight-path angle.

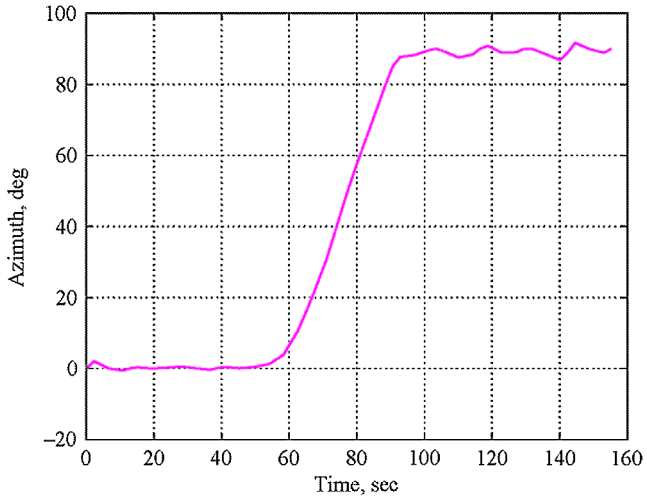

Fig. 11 Time history of azimuth.

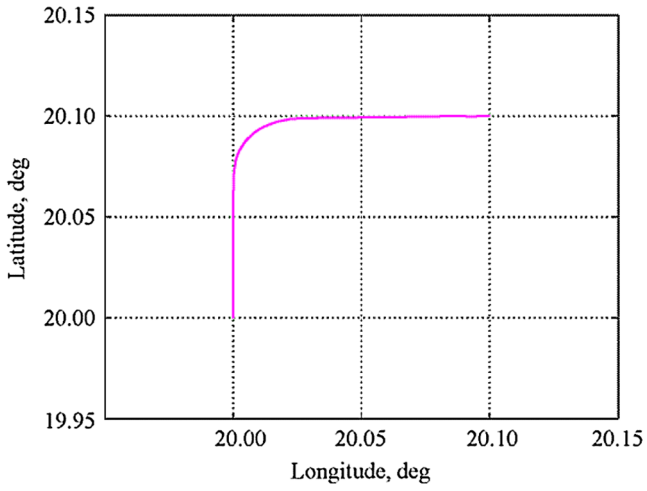

Fig. 12 Latitude vs longitude.

that is, adjustments to a few of the SNOPT performance parameter default values (e.g., minor iteration limit, superbasics limit) were necessary to continue the optimization process. Each subsequent optimization cycle was initialized using the final parameter vector from the previous one until a converged solution was achieved. The total number of iterations necessary for the solution was 1393.

Figures 6–12 show the time histories of the translational state variables (altitude, latitude, longitude, velocity, flight-path angle, and azimuth) of the converged solution during the approach to landing. The azimuth angle (Fig. 11) shows the vehicle flying due north for the first half of the flight, and then due east for the second half. The turn is performed between 60 and 90 s to achieve the final

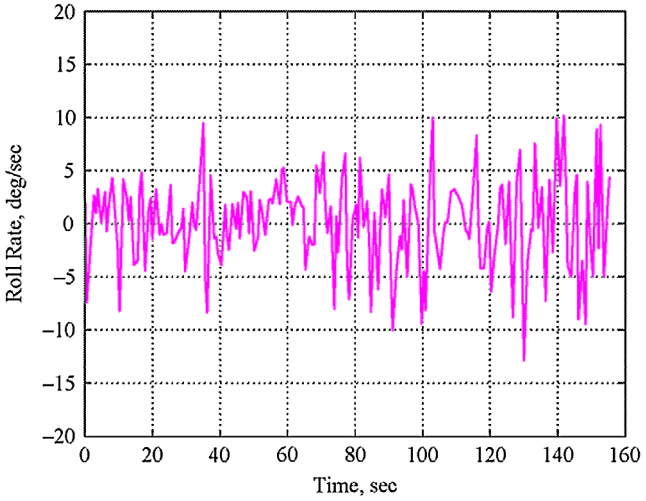

Fig. 13 Time history of roll rate.

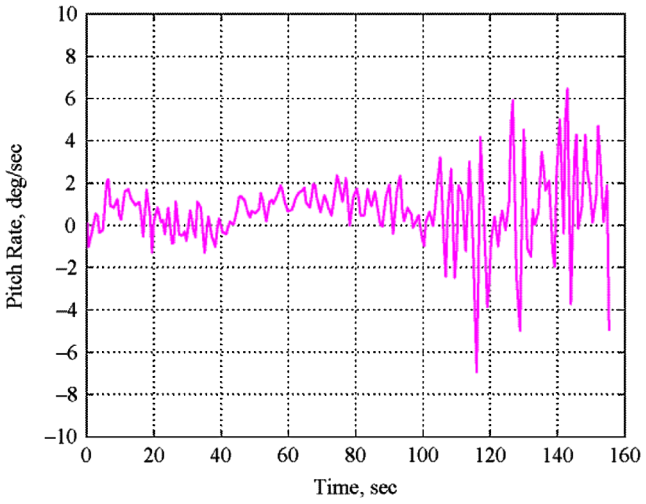

Fig. 14 Time history of pitch rate.

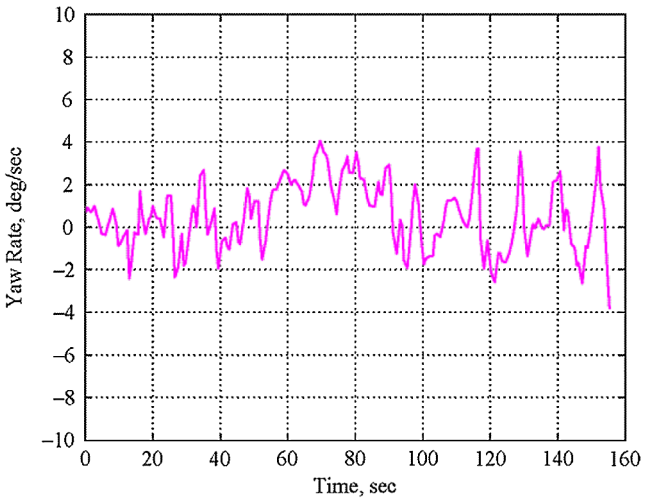

Fig. 15 Time history of yaw rate.

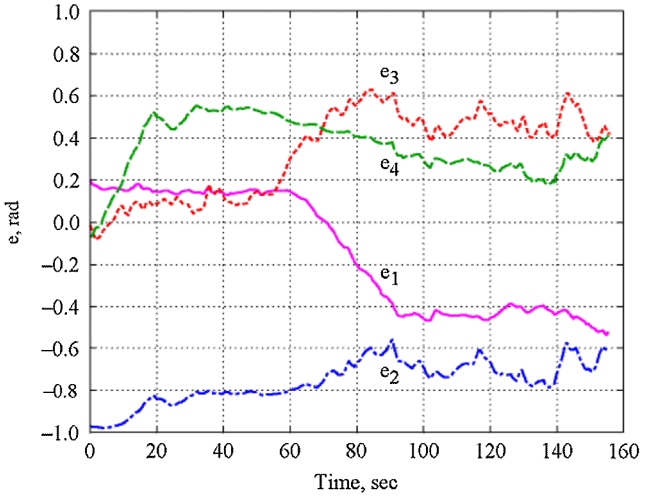

Fig. 16 Time history of quaternion vector.

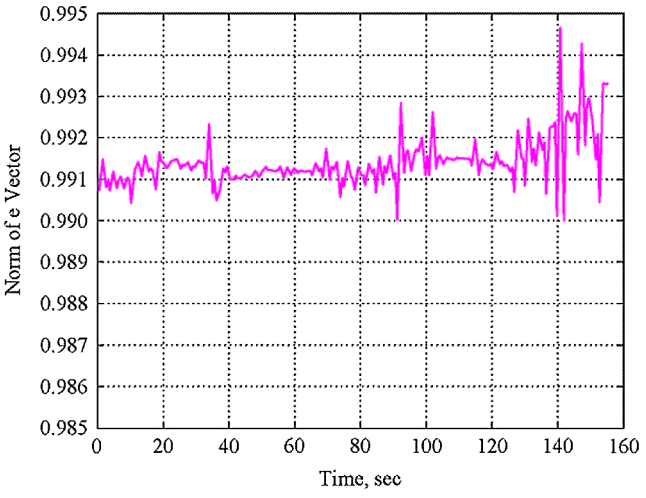

Fig. 17 Time history of quaternion vector norm.

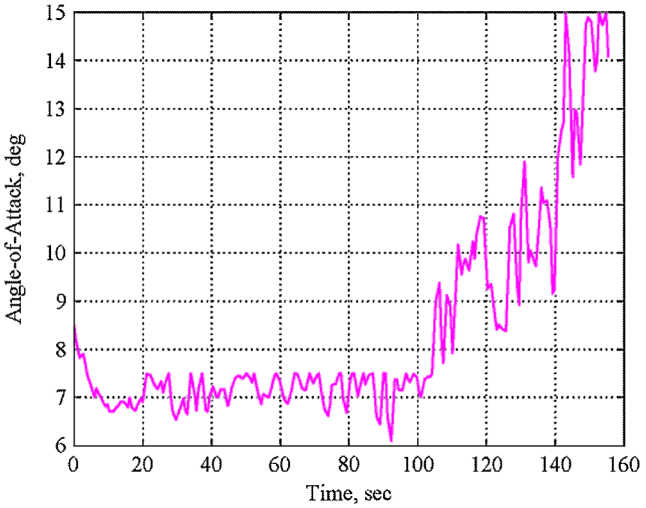

Fig. 18 Time history of angle of attack.

latitude and longitude. The trajectory flown is depicted in Fig. 12. These state variables vary smoothly, exhibiting very low frequency change. Consequently, the number of time segments (12) specified is sufficient to characterize their dynamics, and no additional segments are necessary.

Figures 13–16 show the time histories of the rotational state variables (roll rate, pitch rate, yaw rate, e_1, e_2, e_3, e_4) of the converged solution during the approach to landing. As seen, these state variables exhibit higher-frequency dynamics. The roll, pitch, and yaw rates are fairly small, indicating that the vehicle is not

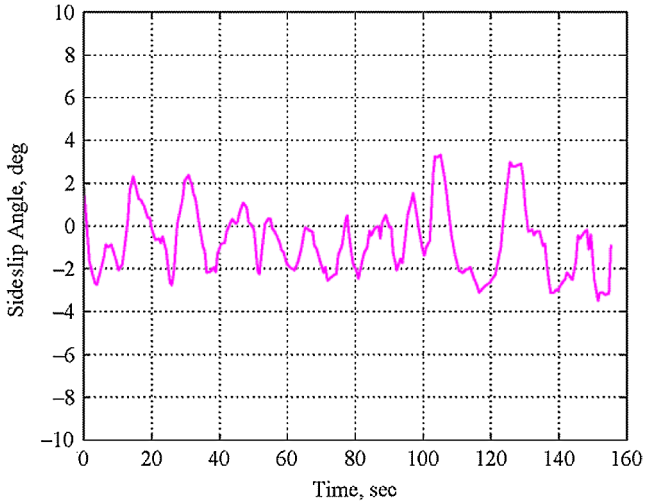

Fig. 19 Time history of sideslip angle.

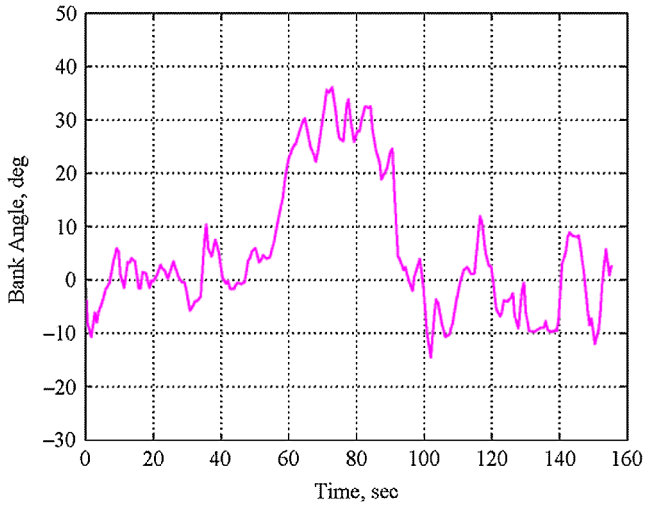

Fig. 20 Time history of bank angle.

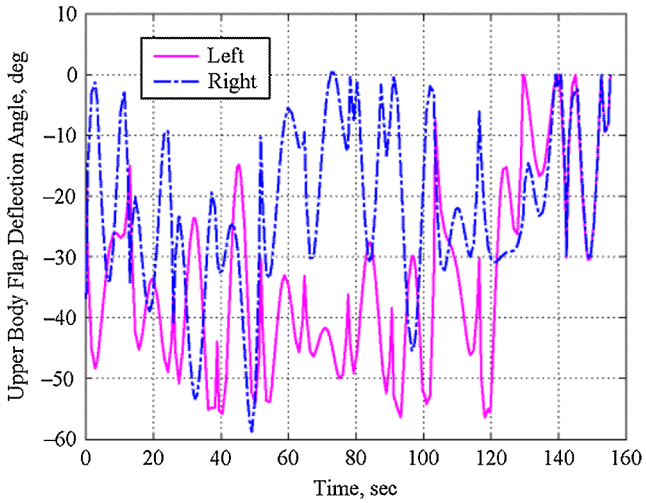

Fig. 21 Time history upper body flap deflection angles.

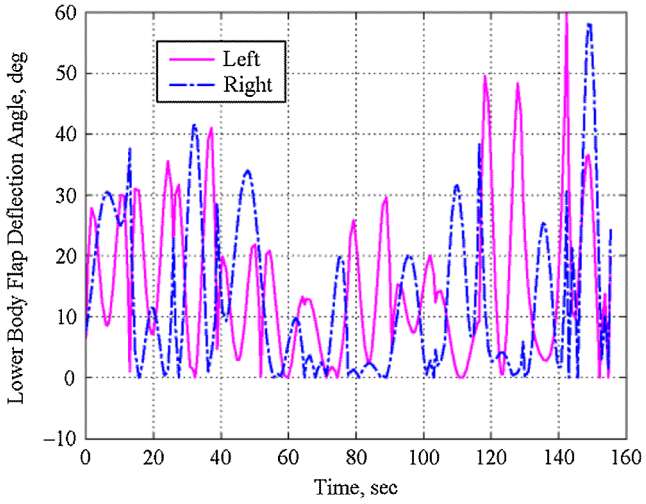

Fig. 22 Time history of lower body flap deflection angles.

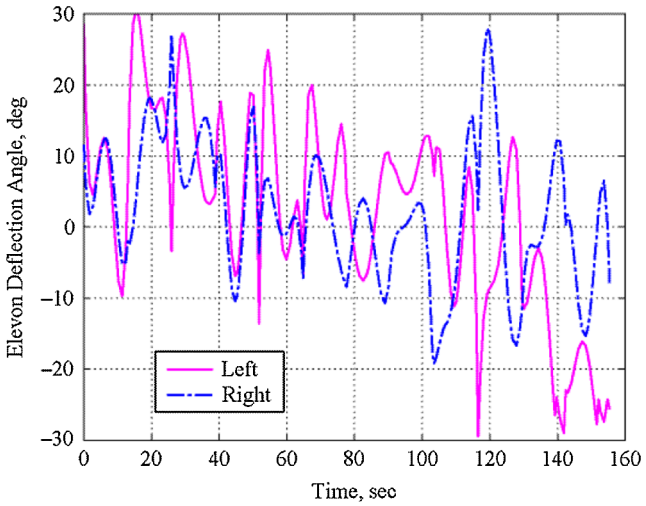

Fig. 23 Time history of elevon deflection angles.

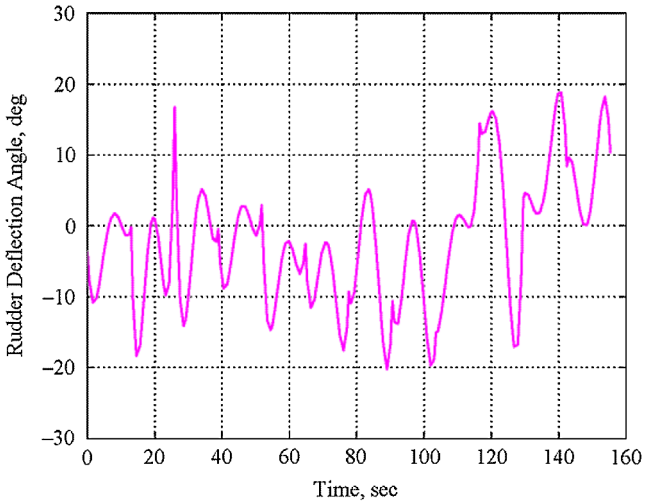

Fig. 24 Time history of rudder deflection angles.

making unrealistically sudden movements. Figure 17 shows the norm of the quaternion vector being near unity, thus satisfying the imposed path constraint. Figures 18–20 show the corresponding attitude behavior of the vehicle in terms of the angle of attack, sideslip, and bank angle, respectively, during the approach and landing. In minimizing the touchdown velocity, the drag on the vehicle is increased during the terminal landing phase by pitching the vehicle to an angle of attack of approximately 15 deg (as seen in Fig. 18). This behavior is typical of the shuttle orbiter, where a flare maneuver is performed shortly before landing to increase drag and

Table 1 Comparison of the standard and four-to-one two-timescale architectures

	No. of segments	No. NLP parameters	No. of constraint equations	No. of elements in Jacobian
Standard	48	2613	1828	4,776,564
Two-timescale	12/48	1173	1396	1,637,508

thus reduce velocity. The sideslip angle is small as would be expected with little sideways attitude. Figure 20 depicts the turn (previously alluded to), where the bank angle increases to approximately 35 deg between 60 and 90 s to align the vehicle heading angle with the runway.

Figures 21–24 show the deflection history of all seven control surfaces (upper left and right body flap, lower left and right body flap, left and right elevon, and rudder).

A solution was attempted for this problem using the conventional standard single-timescale collocation architecture. However, a converged solution was not possible due to the large problem size and the associated difficulties with solving 6DOF problems described previously (i.e., having two distinct timescales, and highly coupled and nonlinear nature of the governing equations). Table 1 summarizes the comparison in problem size between this two-timescale scheme and the single-timescale collocation scheme (which did not yield a solution), both using 48 time segments.

There are a total of 1173 nonlinear variables for the two-timescale scheme, and a total of 1396 nonlinear constraints that need to be satisfied. A large reduction in the overall problem size can be achieved as compared to the standard single-timescale collocation scheme. The number of NLP parameters required is reduced by 55%, whereas a reduction of 22% is seen in the number of constraint equations. The size of the Jacobian matrix is reduced by a significant 66%. Consequently, the two-timescale collocation scheme has demonstrated the capability to solve 6DOF problems with finer discretization resolution than was previously possible using the standard single-timescale collocation scheme. If greater resolution is desired than depicted in the converged solution of this sample test case, the problem can be resolved with more segments.

V. Conclusions

A six-degree-of-freedom approach and landing trajectory optimization problem for a winged vehicle has been successfully solved using a two-timescale collocation architecture. The two-timescale collocation discretization scheme allows for a coarser discretization to be used for smoothly varying state variables and a second finer discretization to be used for state variables having higher-frequency dynamics. This approach allows the size of the overall optimization problem to be reduced significantly.

In the two-timescale collocation architecture, 12 segments are specified for the translational state variables (i.e., low-frequency state variables), whereas 48 segments are used for the rotational states variables (i.e., high-frequency state variables). The converged solution shows a realistic landing profile and is able to capture the appropriate rotational dynamics. With this formulation, a large reduction in the overall problem size is attained as compared to the standard single-timescale collocation scheme. A reduction of 55% is observed in the number of NLP parameters required, whereas a reduction of 22% is seen in the number of nonlinear constraint equations. The resulting size of the Jacobian matrix is reduced by 66%. Consequently, the two-timescale collocation scheme has demonstrated the capability to solve 6DOF problems with finer resolution than was previously possible using the standard single-timescale collocation scheme.

References

[1] Hargraves, C. R., and Paris, S. W., "Direct Trajectory Optimization Using Nonlinear Programming and Collocation," *Journal of Guidance, Control, and Dynamics*, Vol. 10, No. 4, 1987, pp. 338–342. doi:10.2514/3.20223

[2] Desai, P. N., and Conway, B. A., "Two-Timescale Discretization Scheme for Collocation," *Journal of Guidance, Control, and Dynamics* (to be published).

[3] Desai, P. N., "Improved Collocation Methods with Applications to Six-Degree-of-Freedom Trajectory Optimization," Ph.D. Dissertation, Aerospace Engineering Dept., Univ. of Illinois, Urbana-Champaign, IL, 2005.

[4] Freeman, D. C., "HL-20 Personnel Launch System: A Concept Definition Case Study," International Astronautical Federation Paper 92-0856, Aug. 1992.

[5] Powell, R. W., "Six-Degree-of-Freedom Guidance and Control-Entry Analysis of the HL-20," *Journal of Spacecraft and Rockets*, Vol. 30, No. 5, 1993, pp. 537–542. doi:10.2514/3.25563

[6] Vlases, W. G., Paris, S. W., Lajoie, R. M., Martens, P. J., and Hargraves, C. R., "Optimal Trajectories by Implicit Simulation Ver. 2.0 User's Manual," Wright Research and Development Center TR-90-3056, 1990.

[7] Vinh, N. X., Busemann, A., and Culp, R. D., *Hypersonic and Planetary Entry Flight Mechanics*, Univ. of Michigan Press, Ann Arbor, MI, 1980, Chap. 2.

[8] Henderson, D. M., "Euler Angles, Quaternions, and Transformation Matrices," NASA TM-74839, July 1977.

[9] Shuster, M. D., "Survey of Attitude Representations," *Journal of Astronautical Sciences*, Vol. 41, No. 4, 1993, pp. 439–517.

[10] Ware, G. M., and Cruz, C. I., "Aerodynamics Characteristics of the HL-20," *Journal of Spacecraft and Rockets*, Vol. 30, No. 5, 1993, pp. 529–536. doi:10.2514/3.25562

[11] Jackson, E. B., Cruz, C. I., and Ragsdale, W. A., "Real-Time Simulation Model of the HL-20 Lifting Body," NASA TM 107580, July 1992.

[12] Herman, A. L., and Conway, B. A., "Direct Optimization Using Collocation Based on High-Order Gauss-Lobatto Quadrature Rules," *Journal of Guidance, Control, and Dynamics*, Vol. 19, No. 3, 1996, pp. 592–599. doi:10.2514/3.21662

[13] Enright, P. J., and Conway, B. A., "Optimal Finite-Thrust Trajectories Using and Nonlinear Programming," *Journal of Guidance, Control, and Dynamics*, Vol. 14, No. 5, 1991, pp. 981–985. doi:10.2514/3.20739

[14] Herman, A. L., "Improved Collocation Methods with Applications to Direct Trajectory Optimization," Ph.D. Dissertation, Aerospace Engineering Dept., Univ. of Illinois, Urbana-Champaign, IL, 1995.

[15] Gill, P. E., Murray, W., and Saunders, M. A., *User's Guide for SNOPT 5.3: A Fortran Package for Large-Scale Nonlinear Programming*, Dept. of Mathematics, Univ. of California, San Diego, CA, Dec. 1998.